Characterization, processing, and interpretation of weak-motion records of a CFRD dam

Juan M. Barbagelata [i], Anna d'Onofrio [ii], Francisco A. Mingorance [iii], Luca Pagano [ii], and Francesco Silvestri [ii]

i) Ph.D Candidate, Department of Civil, Building and Environmental Engineering, University of Naples Federico II, Naples, Italy.
ii) Professor, Department of Civil, Building and Environmental Engineering, University of Naples Federico II, Naples, Italy.
iii) Professor, Direction of Technological Studies and Research, National University of Cuyo, Mendoza, Argentina.

ABSTRACT

Permanent seismic monitoring plays an essential role in the surveillance of embankment dams in seismically active regions. Weak-motion recordings collected from instruments located along the dam body and abutments provide valuable data sets to identify and characterize the dynamic response of the dam-foundation system at small strain levels. The objective of this work was to summarize the characterization and processing of the acceleration time histories recorded during the operation of an earth dam in Argentina, to identify the main features of its dynamic response. The paper first describes the seismic monitoring system of the dam; then, the records were attributed to seismic events pertaining to distinct seismogenic sources through catalogs of seismicity. It was shown that several seismogenic sources characterized by different types of faulting style, distance and magnitude may affect the dam during its operation. A number of selected records was processed in order to obtain a preliminary description of the dynamic response of the dam-foundation system at low-acceleration amplitudes. The analysis of peak acceleration ratios between the crest and mid-height recording stations revealed the significant influence of asynchronous motion. This aspect was confirmed by the analysis of Fourier's and response spectral ratios, which yielded consistent estimates of the fundamental frequency of the dam-foundation system, notwithstanding the variability of the source mechanisms, and permitted to back-figure a realistic value of the average shear wave velocity of the gravelly soil.

Keywords: seismic monitoring, embankment dam, dynamic characterization, seismicity.

1 INTRODUCTION

A permanent seismic monitoring system in an earth dam plays an essential role in case of strong earthquakes, but also when weak motion phenomena affect the dam. The use of more frequent weak motion records in the characterization of the dynamic response of the dam-foundation system (e.g., Sica & Pagano, 2020) have been growing by the increasing number of dams equipped with sensitive and reliable electronic accelerometers. This paper reports a comprehensive analysis of the weak motion seismic database collected at the Potrerillos Concrete Face Rockfill Dam (CFRD) located in the Central Andes of Argentina, in the north of the Mendoza Province.

Previous studies on the seismic response of the dam (De Cicco et al., 2015; Barbagelata et al., 2022) were carried out based on geotechnical design parameters; the information recorded after almost 20 years of seismic monitoring could help to better identify the dynamic response of the system and to refine its geotechnical model for seismic safety assessments.

The primary objectives of this study include classifying the seismogenic sources responsible for generating low-amplitude ground motions at the dam site and conducting a preliminary identification of the dam response to these events as related to geometry and material properties.

The accelerometric records were selected by referring them to events mapped and classified in different seismicity catalogs. Subsequently, ground motion parameters and spectral ratios were evaluated to identify some fundamental features of the dynamic response of the dam, such as its natural period at small strain levels and the average shear wave velocity.

2 DAM AND SEISMIC MONITORING SYSTEM

Potrerillos Dam was constructed in the 2000-2002 period in the southernmost portion of the Western Precordillera belt, along the Mendoza River valley. The dam is 120m tall over the riverbed and 490m long at the crest, with an upstream and downstream slope of 1.5:1.0 and 1.8:1.0 respectively (Fig. 1). The dam is founded in alluvial material with variable depth overlying a Triassic granite bedrock. The impervious barrier of the dam consists of a cut-off concrete wall in the alluvium joined to a reinforced concrete slab along the upstream slope.

The dam is equipped with a seismic monitoring system comprising four accelerometric stations placed along the dam site: three of them are situated in the dam body at key locations: the crest (C9), mid-height (C7), and toe (C1) along a central transverse section of the dam (Fig.1.b). The fourth station (GMD) is located on the right abutment

of the dam (Fig.1.a).

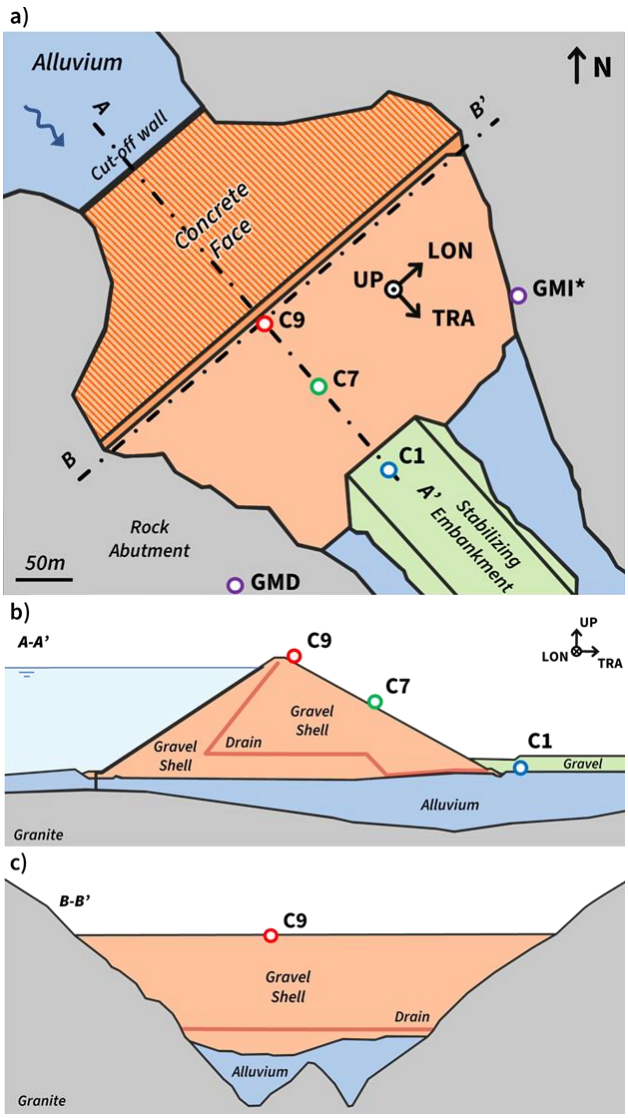

Fig. 1. a) Plan view and main features of the dam with the location of all accelerometric stations, and accelerometer component orientation; b) location of the accelerometric stations along the dam central transverse section; c) dam longitudinal section.

Since the dam completion, the monitoring system underwent two major changes. In 2004 the construction of a stabilizing embankment at the downstream toe of the dam led to the burial of C1 station under a 12m layer of gravel (CEMPPSA, 2007). Later in 2007 the station initially placed on the left abutment (GMI* in Fig.1.a) was repositioned to the entry of a gallery located in the right margin (GMD in Fig. 1.a).

Each station is equipped with a triaxial electronic accelerometer GeoSIG AC-33 with the three components (TRA, LON, UP) oriented as shown in Fig.1. Every instrument is equipped with a GPS to synchronize the recording time of the whole array and it is appropriately placed on a reinforced concrete block independent of the housing that covers it. The accelerometers are connected through an intranet with the main monitoring center, located about 4km away from the dam, from where the instruments settings can be controlled and the signals are logged and collected in a mass memory storage.

For all the instruments, the triggering threshold is set to a_{tr}=0.004g and the full-scale range to ± 2g. The pre-and post-event buffer time lengths are set to 15s and 25s, respectively (Calderón & Cordone, 2019).

3 DATA PROCESSING

The signals recorded from each station were first attributed to the source seismic events and then some selected records were processed to derive useful information about the seismic response of the dam.

Out of a total of 129 earthquakes recorded by at least one station of the monitoring array in the 2002-2021 period, 119 (108 mainshocks and 11 aftershocks) could be accurately linked to their source seismic event. This process involved comparing the starting time of the signals recorded by each station with the assigned in the ISC catalog of seismicity (ISC Bulletin, 2022). Additionally, the local INPRES catalog (INPRES, 2022) was consulted for small-magnitude events.

The focal mechanism was identified for 39 earthquakes characterized by a moment tensor solution in the catalogs CMT (Ekström et al., 2012), ANSS (USGS, 2017) and GFZ (Quinteros et al., 2021). Each event was associated to the main faulting styles characterizing the local seismogenic environment (Jordan et al., 1983), distinguishing shallow crustal (CR), subducted intra-slab (IS) and subduction interface (SD) earthquakes.

For each different faulting mechanism, the couple of events characterized by the highest peak ground acceleration (*PGA*) was then selected. Following the suggestions by Boore & Bommer (2005), baseline correction and bandpass filters were applied to minimize the impact of the noise in the signals for the subsequent interpretation of the dynamic response of the dam.

Table 1 lists the main properties of the six selected events; with reference to the transversal component, the *PGA* and Arias Intensity, *AI*, recorded at the crest, together with the dominant frequency, f_D, of the response spectrum at the abutment are also reported.

Table 1. Properties of the selected events and reference records.

Event	Date	magn. [Mw]	ep.dist. [km]	depth [km]	*PGA* C9 [g]	*AI* C9 [m/s]	f_D GMD [Hz]
CR-01	5/8/2006	5.6	33.7	32.0	0.065	0.0379	5.0
CR-02	23/6/2021	4.6	12.0	19.0	0.094	0.0283	10.0
IS-01	26/4/2009	5.1	33.9	132.0	0.007	0.0003	7.1
IS-02	18/1/2010	5.5	199.6	91.0	0.027	0.0050	3.6
SD-01	27/2/2010	8.8	502.3	22.9	0.024	0.0533	2.3
SD-02	16/9/2015	8.3	287.1	22.4	0.016	0.0326	4.2

From the processed records, ground motion parameters and spectral ratios were derived to characterize the dynamic response of the dam at small strains. The computation of the Standard Spectral Ratio

(*SSR*) and the Ratio of Spectral Acceleration (*RSA*) between ground motions at the crest and the abutment stations was conducted using the following expressions:

$$SSR(f) = \frac{A(f)_{C9}}{A(f)_{GMD}} \quad (1)$$

$$RSA(f) = \frac{Sa(f)_{C9}}{Sa(f)_{GMD}} \quad (2)$$

according to the procedures adopted by Castro et al. (2000) and Armstrong et al. (2021), correspondingly. In Eqs. (1) and (2), *A(f)* and *Sa(f)* stand for the Fourier amplitude and acceleration response spectra, respectively.

The computation of *SSR* was carried out following the time windowing recommended by Mikami et al. (2008), and adopting the moving average algorithm suggested by Konno & Ohmachi (1998) for the spectral smoothing, assuming a bandwidth coefficient *b*=40 to avoid distortions in the peaks of the spectral ratios.

4 RESULTS

4.1 Events distribution

The spatial distribution of the above mentioned 119 seismic events is shown in Fig. 2. Symbols of different colors represent different source types, with their sizes proportional to the moment magnitude (Mw). The epicenter locations are compared with contours indicating the depth of the subducted plate, and focal depths are plotted along a vertical West-East section across the dam site.

It is worth noticing that the couple of SD earthquakes selected in this study (refer to Table 1) correspond to two of the largest events occurred in the past years along the coastal Chilean subduction zone, i.e., the Maule 2010 Mw 8.8 and Illapel 2015 Mw 8.3, which generated ground motions with significant energy content at the dam site, although its large epicentral distance (more than 500km and almost 300km, respectively).

The intra-slab events, mainly situated at the North of the dam, are characterized by higher focal depths; their hypocenters follow an alignment and depths similar to that of the subducted plate (see Fig. 2). The crustal events, located closer to the dam, are characterized by a shallower and sub-horizontal distribution in depth, consequence of the seismotectonic environment derived by the flat-slab subduction regime denoted by the contours of the subducted plate depth in Fig. 2.

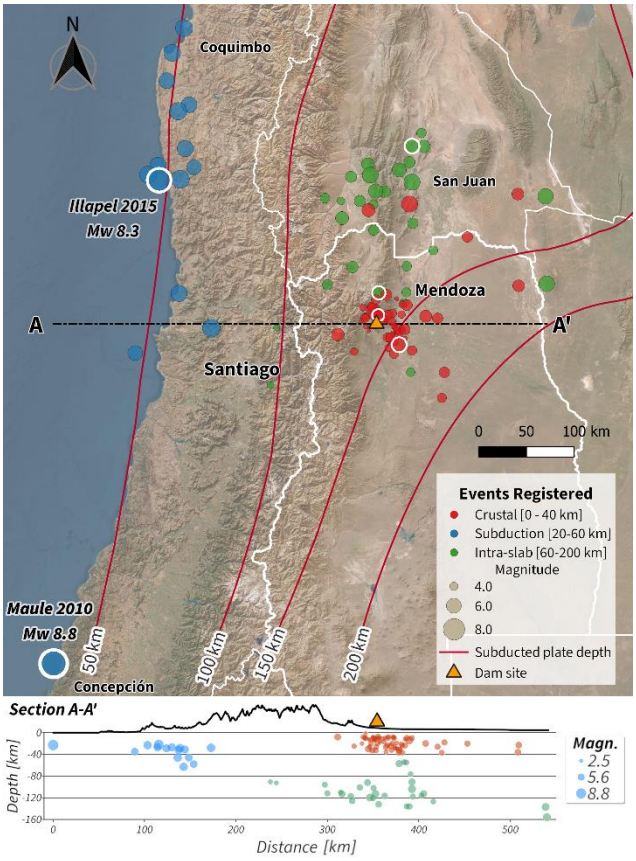

Fig. 2. Distribution of seismic events with records in the dam, with the events of Table 1 emphasized.

The 39 events with a well-identified focal mechanism are plotted in the map of Fig. 3 according to the same color code and symbol size assumed previously.

In Fig. 3, a plot generated by the FMC code (Álvarez-Gómez, 2019) is presented, classifying the events based on focal mechanisms into the three well-known types of fault mechanisms (Reverse, Normal, and Strike-Slip), along with their combinations. The figure reveals that nearly all subduction events correspond to Reverse faulting. Intra-slab events are distributed between Normal or Normal-Strike-Slip mechanisms, while the majority of Crustal events are either Oblique or Reverse

4.2 Dynamic characteristics of the dam

Out of the 119 identified events, 28 were recorded by the GMD/GMI* station, 67 by C1, 117 by C7, and 95 by C9. Additionally, only 21 events were recorded at all the stations, 47 simultaneously recorded at the embankment stations (C1, C7 & C9) and 65 events at the two more elevated and sensitive dam stations (C7 & C9).

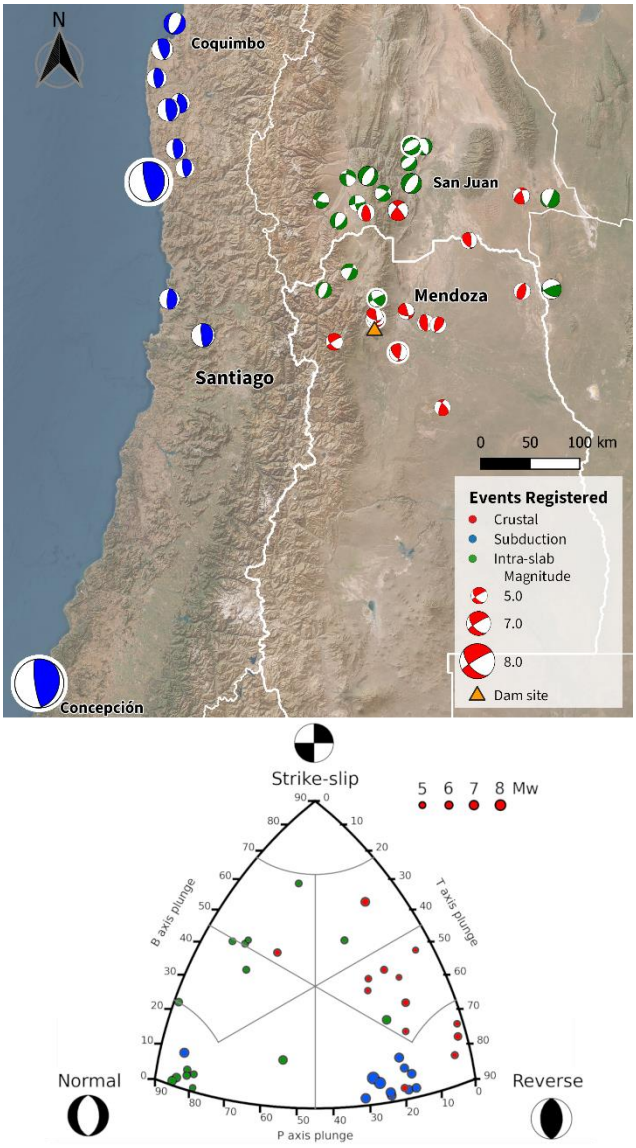

Fig. 3. Geographical distribution and focal mechanism classification of the well-identified events.

The plot in Fig. 4 shows the ratio between the peak ground acceleration recorded at the dam crest (C9) and mid-height (C7) for the TRA and LON components. It can be noted that most data points fall in the green-shaded area, where *PGA* at crest is attenuated with respect to that at mid-height. In detail, this happens for 70% of the records of the transversal component along the embankment section and for 60% of those along the dam axis. This particular response does not show correspondence with a specific type of event since PGA_{C9}/PGA_{C7} ratios greater and smaller than unity were verified to occur for diverse focal mechanisms.

The *SSR* defined by Eq. (1) was employed to identify the dynamic characteristics of the dam using weak motion records, as described in Sica & Pagano (2020). Fig. 5 shows the *SSR* between the TRA components relevant to the three couples of selected events (see Table 1), grouped according to the type of source mechanism.

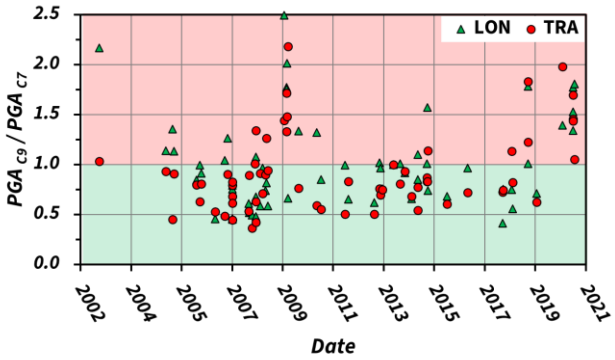

Fig. 4. Ratio between PGA at C9 and C7 for the TRA and LON components.

The predominant peak of the *SSR* is considered as the first natural frequency of the dam-foundation system. It can be noticed regardless the faulting style considered; the selected records consistently indicate that the first natural frequency is around 2Hz. The remaining peaks might be associated to higher modes of vibration, which are not necessarily related to in-plane transversal motion but can arise from the three-dimensional response of the dam.

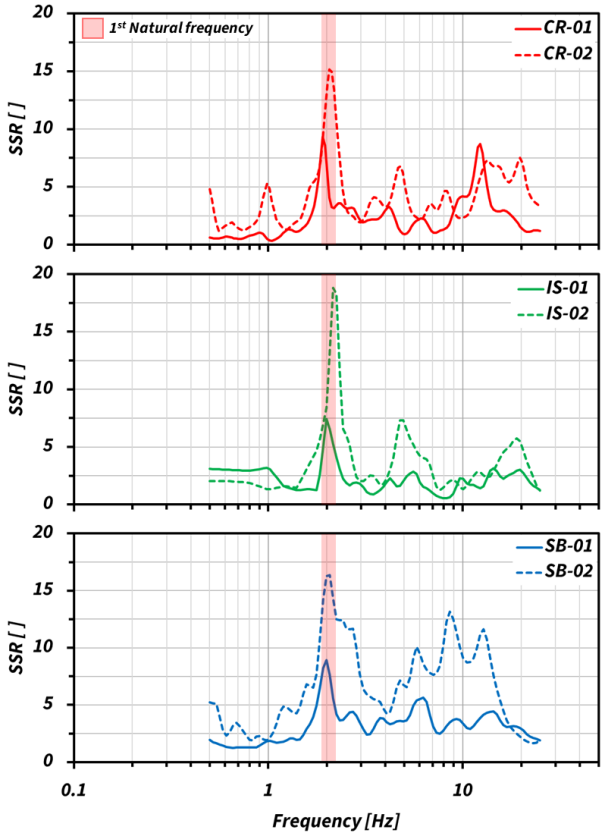

Fig. 5. Standard Spectral Ratio for the main selected records.

The plot in Fig. 6 presents, as an example, the *RSA* computed as defined in Eq. (2) for the case of the TRA component of CR-01 record, by assuming a 5% viscous damping. The double-scale chart permits to verify that the 2Hz peak observed by the *RSA* pertains to the dynamic

response of the dam-foundation system since this peak is not present in the reference motion recorded at the abutment (purple spectrum), while it is apparent at the crest (red spectrum). This finding aligns with the interpretation from the *SSR*, as well as a significant influence of a higher vibration mode around 10.5Hz can be recognized.

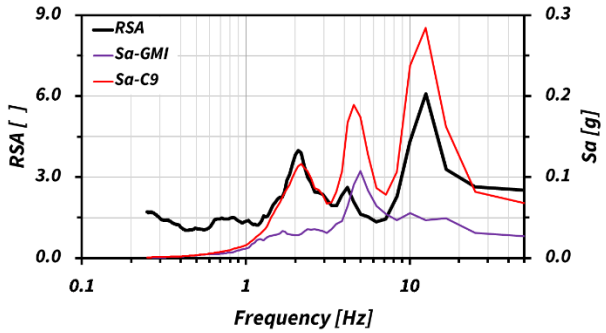

Fig. 6. Ratio of spectral acceleration (*RSA*) and acceleration spectra *Sa* for the C9 and GMD motion (event CR-01, TRA component).

By knowing the natural frequency from the spectral ratios and the main geometrical characteristics of the dam-foundation system, it was possible to back-figure an approximated value of the average shear wave velocity of the gravelly soil, which has never been measured in the embankment insofar. In this study, reference was made to one of the expressions presented in Gazetas & Dakoulas (1992) for the case of triangular-shaped dam laying on a foundation subsoil with comparable properties, both assumed as characterized by a parabolic stiffness profile:

$$f_1 = \frac{V_s}{2.57 \times 0.9 \times H} \tag{3}$$

where 2.57 is the coefficient to be adopted when approximating the 2D response of the dam body to that of an inhomogeneous 1D shear-beam ($V_S \propto z^{1/3}$) and 0.9 is a correcting factor to be used when the foundation subsoil along the dam axis can be approximated with a trapezoidal valley (see Fig.1.c). In this specific case, by assuming H=120m and f_1=2Hz, the average shear wave velocity V_S resulted equal to 555m/s, higher than the value of 424m/s assumed in the previous studies above mentioned on the basis of seismic refraction surveys in trial embankments at the dam site (De Cicco et al., 2015). This inconsistency can be primarily attributed to the different state of confinement and level of lithostatic stresses existing between the trial embankment and the dam.

5 DISCUSSION AND CONCLUSIONS

The analysis of the records from the permanent seismic monitoring system of the Potrerillos dam was exploited for the twofold purpose of:

(i) evaluating the site seismicity, by distinguishing the influence of different seismic sources on the dam response,

(ii) validating or refining the dynamic model of the dam-subsoil system to enhance dam performance prediction during strong-motion earthquakes.

This study provides a preliminary interpretation of the contribution of the three different types of seismic sources whether in the vicinity of the dam or far away, and how they could influence the seismic hazard of the site. On the other hand, the analysis of spectral ratios relevant to clusters of records with different fault styles, magnitudes and distance constituted a valuable tool to identify the natural frequencies of vibration regardless of the signature of the source signal and, subsequently, to back-figure an average value of shear wave velocity, an important parameter for the calibration of numerical models.

The existing literature on this subject is often focused on the identification of the dynamic characteristics of the dam without distinction among the seismic events that triggered the recordings. The careful selection and classification of the seismic records proposed in this study tried not only to bring more information about the seismic sources around the dam site, but also to assess if and how their particular faulting mechanisms could influence the site-specific seismic hazard and the dam response.

Following the analysis of the source mechanisms effects on the signals recorded along the dam, it can be inferred that:

- Large and distant subduction earthquakes do not produce significant shaking amplitudes in the dam site (see Table 1) even when the dominant frequencies recorded at the abutment are close to the dam fundamental frequency (2Hz), due to the attenuation effect resulting from the distance and the presence of the Andean Cordillera mountain chain between the source and site (Barbagelata et al., 2018).
- The Intra-slab events represent a challenging source of seismicity affecting the dam site-specific hazard because the location and size of the events cannot be precisely estimated. Despite the relatively high and slightly variable focal depths on average, a potential earthquake with epicenter close to the dam site is likely and can produce non-negligible ground motion amplitude even with a moderate magnitude.
- Crustal events emerge as the most influential in the dam response from the evaluation of the seismic records considered. In fact, the moderate events recorded at the dam site along the monitoring period show non-negligible *PGA* values, and the seismic potential in the vicinity of the dam can produce larger magnitude events than those recorded (Salomon et al., 2013).

From the comparisons of the signals recorded along the dam, a first result which appears atypical is that in most cases the amplitudes recorded at mid-height of the dam are higher than those at the crest. This apparent anomaly might depend on the combination of the dam-foundation 3D variable geometry and soil properties, leading to a response notably influenced by asynchronism

(Bilotta et al., 2010) associated to higher vibration modes (see Figs. 5-6) which might induce maximum acceleration amplitudes around the middle zone of the dam's height. The presence of asynchronism for the cases where $PGA_{C9}/PGA_{C7} < 1.0$ is supported by the fact that the ratio between the predominant frequency of the reference motion recorded at the abutment (f_D) and the first natural frequency of the dam-subsoil system (f_1) is greater than 1.0 (e.g. CR-01, IS-01 and SD-02 in Table 1).

The fundamental frequency of about 2Hz back-figured from the spectral ratios confirms the results reported by Calderón & Cordone (2019) and constitutes a reference for future works in the calibration of numerical models.

The use of the *SSR* for identifying the natural frequencies of the dam (Fig. 5), demonstrated reliability after applying suitable signal processing procedures. The identified natural frequencies were checked to be independent of the choice of records with variable source mechanisms and distances (refer to Table 1). On the other hand, the use of the *RSA* as an alternative to the *SSR* is an attractive option to identify the natural frequencies of vibration, because it requires an easier procedure, less sensible to correction, filtering, and smoothing techniques.

It must be noted that an empirical estimation of the fundamental frequency of the embankment-foundation system is not applicable in the design stage but limited to existing dams. For these latter, it can represent an affordable, yet reliable, alternative way with respect to the use of numerical simulations or simplified formulae, in order to define the appropriate constraints for the selection of reference input motions required for seismic hazard assessment (Zimmaro & Ausilio, 2020).

Finally, the average shear wave velocity back-figured using Eq. (3) resulted larger than the values used in previous seismic response studies and design analyses, which were based on geophysical investigations on a trial embankment but never supported by direct measurements in the actual dam body.

Future work will be addressed to clarify the role of the variable subsoil conditions underneath the dam, soil nonlinear behavior and 3D dynamic effects in the seismic response of the Potrerillos dam, to exploit the monitoring system as an early warning tool for its safety.

REFERENCES

1) Álvarez-Gómez, J. A. (2019). FMC—Earthquake focal mechanisms data management, cluster and classification. *SoftwareX*, 9, 299–307. https://doi.org/10.1016/j.softx.201 9.03.008
2) Armstrong, R., Kishida, T., & Park, D. (2021). Efficiency of ground motion intensity measures with earthquake-induced earth dam deformations, *Earthquake Spectra*, 37(1), 5–25. https://doi.org/10.1177/8755293020938811
3) Barbagelata, J. M., d'Onofrio, A., & Silvestri, F. (2022). The elastic behavior of two types of embankment dams under seismic loading considering dam-reservoir interaction effects, *Incontro Annuale Dei Ricercatori Geotecnica,* Caserta, Italia, 1-6.
4) Barbagelata, J. M., Iannizzotto, R., & Mingorance, F. (2018). Análisis preliminar de registros de aceleración de dos eventos de subducción en las estaciones acelerográficas del sitio Capdeville, norte de Mendoza,. *I Jornadas de Divulgación de la Carrera de Ingeniería Civil,*. Mendoza, Argentina, 1-5.
5) Bilotta, E., Pagano, L., & Sica, S. (2010). Effect of ground-motion asynchronism on the equivalent acceleration of earth dams. *Soil Dynamics and Earthquake Engineering*, 30(7), 561–579. https://doi.org/10.1016/j.soildyn.2010.01.014
6) Boore, D. M., & Bommer, J. J. (2005). Processing of strong-motion accelerograms: Needs, options and consequences. *Soil Dynamics and Earthquake Engineering*, 25(2), 93–115. https://doi.org/10.1016/j.soildyn.2004.10.007
7) Calderón, F., & Cordone, J. P. (2019). Determinación de la frecuencia fundamental de una presa CFRD mediante funciones de transferencia. *XXI Chilean Conference on Seismology and Eartquake Engineering*, 1-8.
8) Castro, R., Ruiz, E., Uribe, A., & Rebollar, C. (2000). Site Response of the Dam El Infiernillo, Guerrero-Michoacan, Mexico. *Bulletin of the Seismological Society of America*, 90(6), 1446–1453. https://doi.org/10.1785/0119990050
9) CEMPPSA. (2007). Manual de Auscultación — Proyecto Potrerillos. S.A , p. 65.
10) De Cicco, R., Barchiesi, A., & Silvestri, F. (2015). Metodología y herramientas para el diseño sismorresistente de presas tipo CFRD. *VIII Congreso Argentino de Presas y Aprovechamientos Hidroeléctricos*, Santa Fe, Argentina, 1-9.
11) Ekström, G., Nettles, M., & Dziewoński, A. M. (2012). The global CMT project 2004–2010: Centroid-moment tensors for 13,017 earthquakes. *Physics of the Earth and Planetary Interiors*, 200–201, 1–9. https://doi.org/10.1016/j.pepi.2012.04.002
12) Gazetas, G., & Dakoulas, P. (1992). Seismic analysis and design of rockfill dams: State-of-the-art. *Soil Dynamics and Earthquake Engineering*, 11(1), 27–61. https://doi.org/10.1016/0267-7261(92)90024-8
13) INPRES (2022). [dataset]. Catálogo Sísmico, Instituto Nacional de Prevención Sísmica.
14) ISC Bulletin. (2022). [dataset]. International Seismological Centre. https://doi.org/10.31905/D808B830
15) Jordan, T. E., Isacks, B. L., Ramos, V. A., & Allmendinger, R. W. (1983). Mountain Building in the Central Andes. *Episodes*, 6(3), 20–26. https://doi.org/10.18814/epiiugs/1983/v6i3/005
16) Konno, K., & Ohmachi, T. (1998). Ground-motion characteristics estimated from spectral ratio between horizontal and vertical components of microtremor. *Bulletin of the Seismological Society of America*, 88(1), 228–241. https://doi.org/10.1785/BSSA08 80010228
17) Mikami, A., Stewart, J. P., & Kamiyama, M. (2008). Effects of time series analysis protocols on transfer functions calculated from earthquake accelerograms. *Soil Dynamics and Earthquake Engineering*, 28(9), 695–706. https://doi.org/10.1016/ j.soildyn.2007.10.018
18) Quinteros, J., Strollo, A., Evans, P. L., Hanka, W., Heinloo, A., Hemmleb, S., Hillmann, L., Jaeckel, K.-H., Kind, R., Saul, J., Zieke, T., & Tilmann, F. (2021). The GEOFON Program in 2020. *Seismological Research Letters*, 92(3), 1610–1622. https://doi.org /10.1785/0220200415
19) Salomon, E., Schmidt, S., Hetzel, R., Mingorance, F., & Hampel, A. (2013). Repeated Folding during Late Holocene Earthquakes on the La Cal Thrust Fault near Mendoza City (Argentina). *Bulletin of the Seismological Society of America*, 103(2A), 936–949. https://doi.org/10.1785/0120110335
20) Sica, S., & Pagano, L. (2020). On the Role of Weak-Motion Earthquakes Recorded on Earth Dams. *Dam Breach Modelling and Risk Disposal*, 345–356. Springer International Publishing. https://doi.org/10.1007/978-3-030-46351-9_36
21) USGS (2017).[dataset] Advanced National Seismic System Comprehensive Catalog. https://doi.org/10.5066/F7MS3QZH
22) Zimmaro, P., & Ausilio, E. (2020). Numerical Evaluation of Natural Periods and Mode Shapes of Earth Dams for Probabilistic Seismic Hazard Analysis Applications. *Geosciences*, 10(12), 499. https://doi.org/10.3390/geosciences10120499